ELSEVIER

Journal of Power Sources 94 (2001) 122–128

JOURNAL OF POWER SOURCES

www.elsevier.com/locate/jpowsour

Short communication

Key factors controlling the electrochemical performance of the cation-deficient mixed spinel oxide $Mn_{2.2}Co_{0.27}O_4$ as cathode in 3 V rechargeable lithium batteries

P. Lavela[a], L. Sánchez[a], J.L. Tirado[a], S. Bach[b,*], J.P. Pereira-Ramos[b]

[a]*Laboratorio de Química Inorgánica, Facultad de Ciencias, Universidad de Córdoba, Avda. S. Alberto Magno, 14004 Córdoba, Spain*
[b]*Laboratoire d Electrochimie, Catalyse et Synthèse Organique, LECSO-CNRS UMR 7582, 2 rue Henri Dunant, 94320 Thiais, France*

Received 8 May 2000; accepted 2 October 2000

Abstract

The synthesis and the structural features of a mixed manganese-cobalt oxide, $Mn_{2.2}Co_{0.27}O_4$ obtained at low temperature (400°C) are reported. Electrochemical lithium insertion occurs in one reduction process located around 2.8 V, involving only the reduction of manganese ions in the oxide. During cycling experiments, performed with various experimental conditions, the best results show a high capacity retention, i.e. 85% of the initial specific capacity (95 A h/kg) after the 20th cycle. © 2001 Elsevier Science B.V. All rights reserved.

Keywords: Manganese mixed oxides; Cation deficient spinels; Rechargeable lithium batteries

1. Introduction

Lithium manganese ternary oxide has been extensively studied as a positive electrode active material in 4 and 3 V lithium rechargeable batteries [1–7]. When these materials are used as the positive electrode in 3 V lithium secondary cells, a poor cycling behavior is observed, which is mainly due to the negative effects of the Jahn–Teller distortion on lattice stability during continuous changes in Mn(III) content. One approach to overcome these problems and to suppress the Jahn–Teller effect is to replace partially Mn by other transition metals. For example, Co-containing spinels have been the subject of recent studies in an effort to improve the cycling performance [8–11]. We have also demonstrated the interest of a low temperature technique in the synthesis of cation-deficient mixed Mn-Co oxides with spinel structure [12], isostructural of tetragonal Mn_3O_4. These solids may act as host lattices and differ from the conventional Mn_3O_4 structure by the existence of larger number of cation vacancies combined with a high oxidation state of manganese: larger than 3+ on average. Such characteristics cannot be achieved with stoichiometric phase. The presence of cobalt ions in the spinel framework helps to avoid the Jahn–Teller effect, and no structural degradation is observed during the reversible lithium insertion/extraction process in the host lattice. Nevertheless, the cycling galvanostatic experiments in the potential window 4.0/2.0 V show a low capacity retention after the first 20 cycles (56%) for this Mn-Co spinel oxide [11]. Such a poor performance was probably a consequence of the low Li diffusivity found in a wide Li composition range. On the other hand, from low sweep rate cyclic voltammetric measurements, a better rechargeability could have been expected for this compound [11].

To gain a better understanding of the consequences associated with Mn substitution by cobalt, the objectives of this study are to investigate the electrochemical behavior of a cation-deficient manganese-cobalt oxide, $Mn_{2.2}Co_{0.27}O_4$. Several experimental conditions susceptible of optimization are changed, such as the use of flooded or starved Li cells, the potential window, and the proportion of the conducting agent, with the aim of improving the cycling life of the cathodic material. A discussion concerning the experimental conditions required for the design of lithium nonaqueous cells using this active material, $Mn_{2.2}Co_{0.27}O_4$, is presented.

2. Experimental

The Mn-Co oxide was obtained from the thermal decomposition of the corresponding mixed carbonate at 400°C in

* Corresponding author. Tel.: +1-49-78-12-00; fax: +1-49-78-13-23.
E-mail address: bach@glvt-cnrs.fr (S. Bach).

PII: S0378-7753(00)00631-5

static air atmosphere for 1 h. Previously, the mixed manganese carbonate was prepared by the addition of a 1 M aqueous solution of $NaHCO_3$ to a 0.5 M solution of divalent Mn^{2+} and Co^{2+} under continuous flow of CO_2. In both cases, the stoichiometry was confirmed by atomic absorption spectrometry.

The average oxidation state, Z_{Mn}, of manganese in the sample was determined by the following procedure. The sample (ca. 50–100 mg) was dissolved in 50 cm^3 of concentrated H_2SO_4, 50 cm^3 of H_2O and in presence of an excess of ferrous(II) ammonium sulphate until complete dissolution. After cooling to 20–25°C, the excess of ferrous(II) ammonium sulphate is potentiometrically titrated with potassium permanganate. At the same time, a blank is run under identical conditions. The redox and chemical analysis indicate the simultaneous presence of 0.6 Mn^{4+} and 1.6 Mn^{3+} ions (mean oxidation state of Mn, $Z = 3.27$), assuming the presence of Co^{3+} [12]. A convenient formula for this compound is: $\square_{0.53}Mn_{1.6}{}^{3+}Mn_{0.6}{}^{4+}Co_{0.27}{}^{3+}O_4$, the symbol $\square$ corresponds to the vacancies in the oxide which make this solid depart from an Mn_3O_4 stoichiometry.

The XRD data were obtained with a Siemens D-5000 X-ray diffractometer using Cu Kα radiation and graphite monochromator.

Electrochemical studies were alternatively carried out in two-electrode Swagelok (Fig. 1A) and three-electrode glass cells (Fig. 1B). The Swagelok cell was prepared inside the dry box by placing a clean lithium metal disk (7 mm diameter), a glass-fiber separator soaked with the electrolytic solution, and the cathode pellet into a Teflon container with two stainless steel plungers. Concerning the three-electrode glass cell (Fig. 1B), a lithium wire in a separated compartment was used as reference and auxiliary electrodes. The working electrode consisted of a stainless steel grid on which the cathodic material was pressed. The cathode was made in two different compositions: (i) a mixture of active material (80 wt.%) with graphite (7.5 wt.%), acetylene black (7.5 wt.%) and PTFE (5 wt.%), or (ii) a mixture of active material with graphite (90–50 wt.%). The electrolyte used was 1 M $LiClO_4$, previously dried under vacuum at 170°C for 16 h, dissolved in distilled propylene carbonate (PC).

Unless otherwise specified, the cathodes were cycled at *C*/2 rate within a 4.0–2.0 V potential window in Swagelok cells, which were controlled by a MacPile I potentiostat-galvanostat.

3. Results and discussion

Chronopotentiometric curves for the reduction and oxidation process at constant current of the cation-deficient spinel oxide $Mn_{2.2}Co_{0.27}O_4$ are reported in Fig. 2, for which a proportion of additives frequently used in our electrochemical experiments (7.5% carbon black, 7.5% graphite, and 5% PTFE) and a two-electrode Swagelok-type cells were used. Irrespective of cycling rate, a main reduction step is located around 2.8 V (Fig. 2A). This transfer of charge involves only manganese ions in the cation-deficient spinel oxides [11], and on account of the initial Mn^{4+} content available, this electrochemical reaction implies that Mn^{4+} and Mn^{3+} ions are reduced at not a very dissimilar cell potential. The differential capacity curves discussed below will throw light on this question. On the contrary, two quasi-plateaux are clearly observed at ca. 3.0 and 3.5 V during the charge of the cathodes, which are best resolved at low currents.

The examination of the first 20 cycles performed at different rates makes evident a lower capacity (0.5 F/mol) for that sample recorded at the higher rate (Fig. 2B). The values of capacity retention at the 20th cycle were calculated with respect to the first cycle capacity (R_{20}). In general, low values around 50% were obtained. In spite of it, the higher value corresponds to the cell discharged at *C*/2. This effect can be interpreted in terms of several concurrent factors, such as: (i) electrolyte evaporation or degradation that could occur mainly in cathodes cycled at low rates, which require a long time to achieve a large number of cycles, or (ii) the influence of the constant voltage regions during charging, that could be responsible for a high polarization in the curves during the oxidation process, as shown in Fig. 2A. The coexistence of several intermediate phases with different lithium contents is known to be the origin of these plateaus during the redox process. Such hindrance to the alkaline ion diffusion into the structure may provoke a structural breakdown which is only reflected for a large number of cycles.

In order to improve these results, new experiments were designed in which the above drawbacks were taken into account. In this sense, a glass type cell in which changes in electrolyte volume could be visually detected, a higher volume of electrolyte of 20 cm^3, and a new ratio of additives were chosen. The results of cell capacity versus cycle number are displayed in Fig. 3. Thus, higher capacities for a large number of cycles were obtained in cathodes built in an elevated proportion of graphite. These results agree fairly well with capacity retention. An increase in the value of R_{20}, from 49 to 61%, was obtained for cathodes with a content of 50 and 90% of graphite, respectively. On the other hand, the cell type seems to be a critical factor, not being necessarily an excess of electrolyte to achieve the higher capacities. In fact, the cycling experience performed in Swagelok cell gave rise to improved electrochemical behavior. The capacity loss is reduced to 30%, and a delivered capacity around 90 A h/kg account for the discharge process in the 20th cycle. Hence, huge quantities of graphite, which does not intercalate lithium at the work potential, have shown to enhance the cell performance.

In order to understand these relevant results about the influence of graphite on specific capacity, XRD diffraction studies were carried out in pure $Mn_{2.2}Co_{0.27}O_4$ cathodes before and after the electrochemical lithium insertion. From the XRD data reported in Fig. 4A, the mixed oxide exhibits a

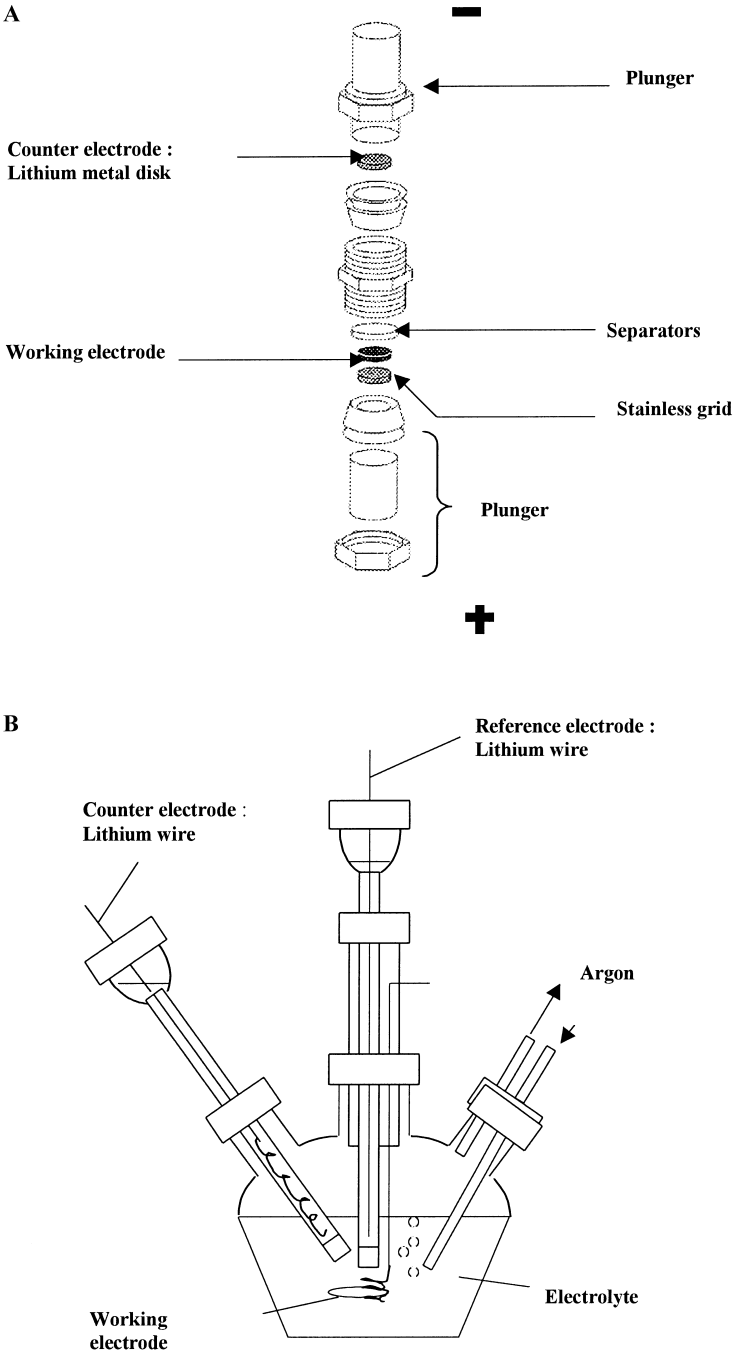

Fig. 1. Schematic representation of Swagelok cell (A) and three-electrode cell (B).

tetragonal spinel structure isotopic with Mn_3O_4 ($I4_1/amd$ space group) with the following cell parameters: $a = 5.72(1)$ Å, $c = 9.30(2)$ Å. The markedly broadened diffraction peaks are consistent with low crystallinity in the particles resulting from the low-temperature synthesis procedure [12]. The cathode used in these electrochemical tests was only composed of active material with the aim of obtaining well resolved X-ray diffraction patterns. In the absence of graphite, the low electronic conductivity in the composite cathode explains the low amounts of Li^+ ions than can be inserted or extracted in these experiments. From the XRD pattern, it can be seen that the structure of the tetragonal phase is largely retained after insertion owing to the rigid 3-D lattice provided by the spinel structure, as it was expected by the presence of cobalt ions in the host lattice. A linewidth decrease of the three main *hkl* reflections — 1 1 2, 0 1 3, and 1 2 1 — was observed in the $Li_{0.55}Mn_{2.2-}Co_{0.27}O_4$ sample (Fig. 4B).

The particularly marked decrease in 1 2 1 line broadening, which is observed from the initial spinel phase to the electrode material after the first discharge could also have its origin in the possible splitting of 1 2 1 and 0 2 2

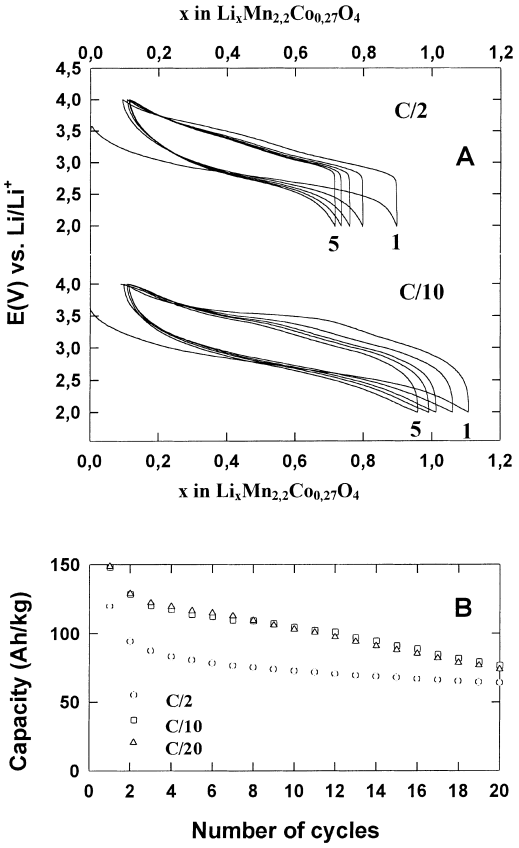

Fig. 2. (A) Discharge/charge profile, and (B) delivered specific capacity corresponding to $Li/Mn_{2.2}Co_{0.27}O_4$ cells cycled at different discharge rates.

profiles which overlap to some extent. Fig. 4C shows a plot of the ratio between both spacings as a function of *c/a*. For the undistorted cubic spinel structure, the pseudotetragonal parameters lead to an axis ratio of $2^{1/2}$, while the exact overlap of both profiles, i.e. d(1 2 1)/d(0 2 2) = 1, takes place for an axis ratio of $3^{1/2}$. Thus, the broadening should decrease on increasing the tetragonal distortion, which in turn is a consequence of a higher content in Mn(III). However, if the *c/a* ratios of pristine spinel (1.63) and discharged materials are compared, little differences can be derived. This is an interesting result which is probably indicative of the simultaneous reduction of Mn(IV) and Mn(III) leading to a nearly constant Mn(III) content. Thus, the Mn(III) content and henceforth the extension of the tetragonal distortion are preserved during discharge. Such situation may have positive effects on capacity retention by limiting the adaptation of the particles to lattice distortions.

From the above discussion, it can be derived that the lithium insertion process causes an increase in the size of the coherently diffracting domains, that can be interpreted as an increase in the crystallite size. The XRD pattern obtained corresponding to a cathode in which five electrochemical discharge/charge processes were made (Fig. 4A), shows a closer similarity with that of the original sample, as a

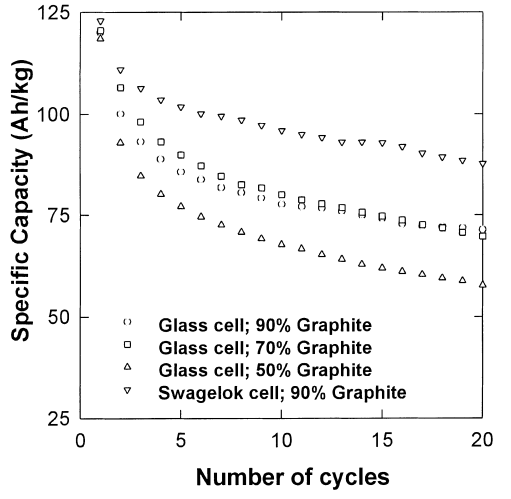

Fig. 3. Specific capacity delivered on cycling by $Li/Mn_{2.2}Co_{0.27}O_4$ cells with different cathode compositions.

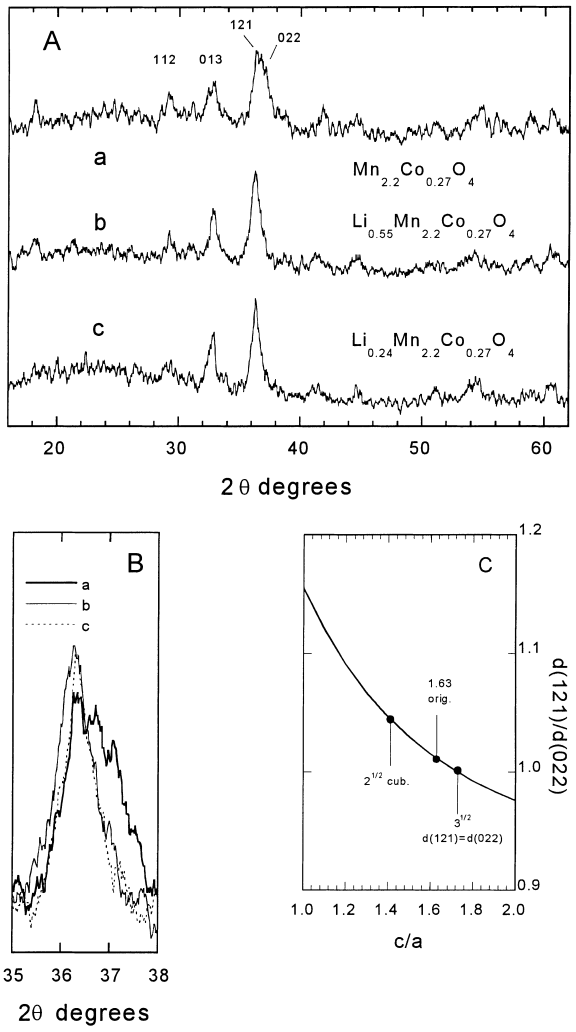

Fig. 4. (A) X-ray diffraction patterns of $Mn_{2.2}Co_{0.27}O_4$ (a), $Mn_{2.2}Co_{0.27}O_4$ after a discharge process until 2.0 V (b), and $Mn_{2.2}Co_{0.27}O_4$ sample after the fifth discharge/charge cycle in the 4.0–2.0 V potential window (c); (B) 1 2 1–0 2 2 *hkl* reflections for the three samples; (C) ratio between 1 2 1 and 0 2 2 spacings as a function of *c/a*.

consequence of its lower lithium content, $Li_{0.24}Mn_{2.2}Co_{0.27}O_4$.

Additional information about the crystallite size can be obtained by the use of the Scherrer equation [13]. Due to low crystallinity of the samples, it was not possible to apply this study to all the *hkl* reflections, and only the data corresponding to the three main *hkl* reflections are written in Table 1. As we can observed, the insertion of Li^+ ions in the spinel structure promotes the increase of the crystallite size. Conversely, this parameter decreases during the lithium extraction process. Significant unit cell volume change was not observed during the above commented electrochemical processes.

The continuous change in crystallite size, which assists in the reversibility of the subsequent lithium insertion/extraction reactions, could be pointed out as one of the key factors that causes the loss of the cell capacity during cycling. The presence of mechanical stress between particles, when the crystallite size increases, would cause the origin of cracking and crumbling phenomena in the cathode. A big dispersion of the active material within the additives helps to avoid the above mentioned phenomena, and leads to a better electrochemical performance of the cathode. This explanation agrees well with the electrochemical behavior observed in Fig. 5. A better capacity retention is obtained from (i) cathodes which have a high additive/active material ratio and cycled at high rate, and (ii) cathodes assembled in two-electrode Swagelok cells. The compact design of the Swagelok cell mitigates the crumbling in the cathode in an easier way than that of three-electrode glass cell. In the former cell, the cathode is compressed between the working and counter electrodes, conversely, in the glass cell the cathode is submerged in a large amount of electrolyte.

Plots of differential specific capacities are useful tools for analyzing the reversibility of an electrochemical oxidation–reduction process. In these type of plots, the plateaux becomes peak, which can be clearly assigned to energetic process occurring during lithium insertion/extraction [14]. Differential specific capacities, dq/m dV, in units of A h/g V, were calculated from adjacent points in the potential–time data ($V(n)$, $V(n+1)$; $t(n)$, $t(n+1)$) using the known value of the current, I, and the active electrode mass, m, as follows:

$$\frac{\mathrm{d}q}{m\,\mathrm{d}V} = \frac{I[t(n+1) - t(n)]}{\{m[V(n+1) - V(n)]\}} \quad (1)$$

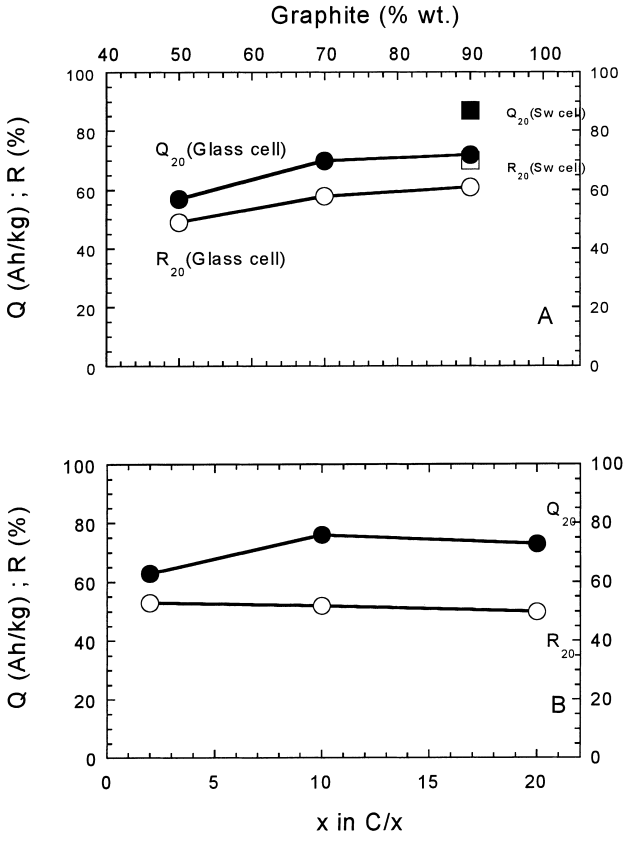

Fig. 5. Capacity retention R_{20} (○) and delivered capacity Q_{20} (●) obtained from: (A) $Mn_{2.2}Co_{0.27}O_4$/graphite cathode with different compositions of graphite and cells configuration; (B) $Mn_{2.2}Co_{0.27}O_4$+ graphite (7.5 wt.%) + acetylene black (7.5 wt.%) + PTFE (5 wt.%) cathode at different *C*/time rates in a Swagelok cell.

Unchanged profiles of the anodic and cathodic derivatives curves on cycling indicate a reversible lithium insertion–extraction process. Fig. 6 shows the dq/(m dV) versus potential plots for the first, fifth, tenth, twentieth and fiftieth discharge–charge sequence of Li/$Mn_{2.2}Co_{0.27}O_4$ cells between 4.0–2.0 V. A broadened cathodic peak was observed at 2.8 V with a shoulder located at 2.6 V. This peak is representative of the successively $Mn^{4+} \rightarrow Mn^{3+} \rightarrow Mn^{2+}$ reducing process. In the anodic part of the plot, two peaks are observed at 3.0 and 3.7 V potential values, which correspond to the $Mn^{2+} \rightarrow Mn^{3+}$, and $Mn^{3+} \rightarrow Mn^{4+}$ oxidation processes, respectively. After

Table 1
Cell parameters and crystallite size values for $Mn_{2.2}Co_{0.27}O_4$

Sample	Composition	a (Å)	c (Å)	V (Å^3)	L (Å) 1 1 2	L (Å) 0 1 3	L (Å) 1 2 1
(a)[a]	$Mn_{2.2}Co_{0.27}O_4$	5.72(1)	9.30(2)	304.3	283	127	85
(b)[b]	$Li_{0.55}Mn_{2.2}Co_{0.27}O_4$	5.74(1)	9.29(2)	306.1	289	255	157
(c)[c]	$Li_{0.24}Mn_{2.2}Co_{0.27}O_4$	5.728(5)	9.31(1)	305.4	125	200	207

[a] As pristine.
[b] After and electrochemical discharge process up to 2.0 V.
[c] Five discharge/charge process in the 4.0–2.0 V potential window.

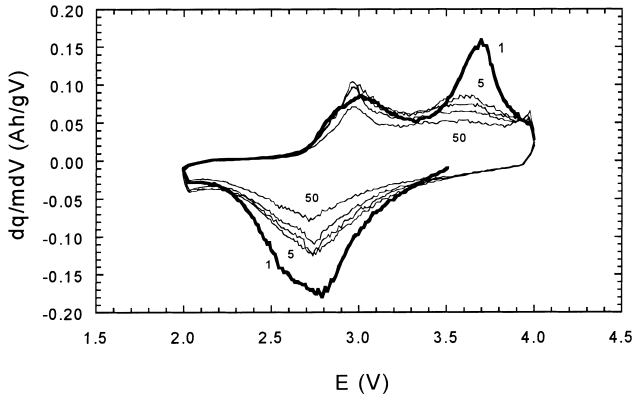

Fig. 6. Differential specific capacity vs. potential for a Li/($Mn_{2.2}Co_{0.27}O_4$/graphite (90 wt.%)) two-electrode Swagelok cell.

several discharge/charge processes are completed, the anodic peak located at 3.7 V tends to disappear, indicating the difficulty for reaccommodating the Mn^{4+} ions into the spinel structure. Hence, a reversible $Mn^{3+} \rightarrow Mn^{2+}$ charge transfer occurs mainly during the lithium insertion/extraction process. This phenomenon may explain the capacity fade found in Li/$Mn_{2.2}Co_{0.27}O_4$ cells. Unfortunately, the very low crystallinity of the intercalated samples did not allowed us to carry out more complete structural studies in order to assign the Mn^{n+} positions.

Additionally, different cell potential windows have been used with the aim to find the best electrochemical performance of Li/$Mn_{2.2}Co_{0.27}O_4$ cells, as it is shown in Fig. 7. The evolution in the electrochemical properties of the cell can be observed when the upper cut-off potential is changed. A better performance is obtained for a cut-off 4.0 V potential, in which the extraction process is near to be completed, and the reoxidation of manganese ions is justified, according to Figs. 2 and 5, respectively. Lower capacity values were recorded using 3.7 V, probably by an incomplete extraction

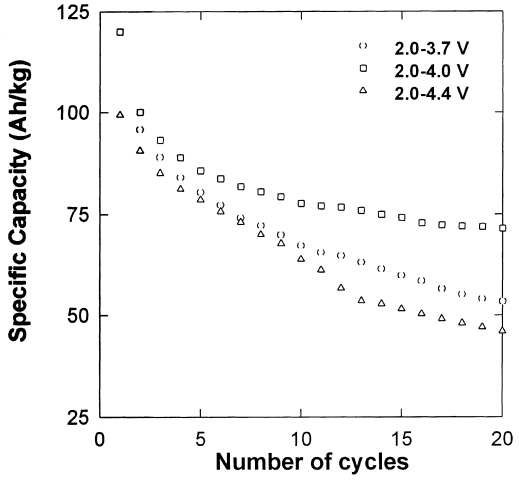

Fig. 7. Specific capacity delivered by Li/($Mn_{2.2}Co_{0.27}O_4$/graphite (90 wt.%)) cells cycled at different potential windows.

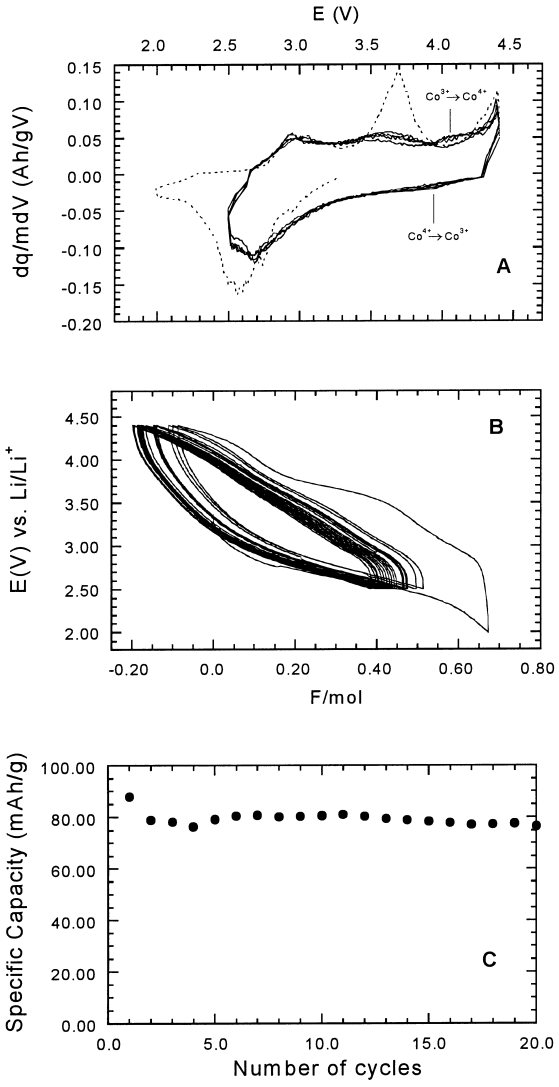

Fig. 8. Differential specific capacity vs. potential (A), charge/discharge profiles (B), and discharge capacity vs. cycles (C) of a Li/($Mn_{2.2}Co_{0.27}O_4$/graphite (90 wt.%)) two-electrode Swagelok cell, corresponding to the first 20 cycles in the 4.4–2.5 V potential window.

process, as mentioned earlier. For a 4.4 V cut-off potential, higher capacities are then expected.

In order to gain capacity while minimizing capacity losses, the differential specific capacity versus cell potential plot was recorded between 2.0–4.4 V for the first cycle, and 2.5–4.4 V for the successive ones (Fig. 8). A sharp and irreversible peak can be regarded at the upper cut-off voltage, which may be induced by non-reversible reactions, such as electrolyte degradation (Fig. 8A). However, this signal decreases for further cycles. At the same time, a new weak band placed at ca. 4.1 V appears in the fitfh cycle whose reversibility is well established in the reduction process by the location of a flat band at ca. 3.9 V. The difference in cell potential from charge to discharge is clearly lower than that of manganese charge transfer described above. The location of these effects on the curve could be explained by the occurrence of $Co^{3+} \rightarrow Co^{4+}$

redox reaction, which in another solids such as $LiCoO_2$, takes place at similar voltages. This effect would justify the overcharge of ca. 0.1 F/mol during the first cycle (Fig. 8B).

For the development of an optimal lithium insertion/extraction electrochemical process, it is necessary to concentrate in the reversible $Mn^{4+} \rightarrow Mn^{3+}$ and $Co^{3+} \rightarrow Co^{4+}$ reactions. The best electrochemical behavior for the Li/$Mn_{2.2}Co_{0.27}O_4$ cell was definitively obtained with a mixture active material/graphite (90 wt.%) as cathode, assembled in a two-electrode Swagelok cell and cycled in a 4.4–2.5 V potential window (Fig. 8B). The corresponding $dq/m\,dV$ versus potential plot is show in Fig. 8A, in which a cathodic peak, located at 2.7 V, and three anodic peaks located at 2.95, 3.7, and 4.1 V are observed. When the Li/$Mn_{2.2}Co_{0.27}O_4$ cell operates at potentials higher than 4.0 V, the reversibility of the new peaks allows us to counteract the initial loss of capacity, caused by using a low reduction cut-off potential, with the gain of capacity obtained when the higher oxidation potential limit is used. Moreover, it has been reported that the additional structural stability supported by the presence of cobalt atoms, which counteracts the negative influence of the Jahn–Teller effects on the structure. Nevertheless, the best result obtained from a lower limit of 2.5 V may arise from a less pronounced dissolution of the oxide material in the electrolyte, leading to manganese and cobalt ions in the solution. This cell shows a high retention of the initial developed capacity (85%) and a constant value of 80 A h/kg for the specific capacity developed in the first 20 cycles (Fig. 8C). The presence of cobalt has been considered as key of structural stabilization [11]. In our case, the electrochemical results obtained here make evident that reversible reduction and oxidation of cobalt ions allow the increase of cell potential up to 4.4 V in order to counteract the capacity fade by cycling the cell under 2.5 V.

4. Conclusions

$Mn_{2.2}Co_{0.27}O_4$ is a member of a large family of lithium-free cation-deficient spinel oxides, which have shown interesting lithium insertion properties which make them potential candidates for lithium battery technology. The mechanism of insertion in these solids has been the subject of extensive works in the past. However, the performance obtained until now was limited by significant capacity losses upon cycling. The optimization of the design of the electrochemical cells, as well as the compositions of the cathodes, as referred to the nature and concentration of the different additives deserves a profound analysis that could facilitate to overcome the intrinsic but avoidable limitations of these materials.

- From a comparative study of the electrochemical behavior in two different cells — a three-electrode cell with flooded electrolyte and a two-electrode cell with a compact design — the interest of the latter is highlighted. This fact could be assumed as a result of decreasing the crumbling of the cathodic material.
- Concerning additives, it was found that the use of large amounts of commercial graphite improves the cycling performance of these materials.
- Regarding the potential window used, it should be remarked that the presence of Co^{3+} ions stabilizes the spinel structure and extends the electrochemical reversible process to the Co^{3+}/Co^{4+} redox pair, around 4 V. In consequence, favoring the $Mn^{4+} \Leftrightarrow Mn^{3+}$ versus the $Mn^{3+} \Leftrightarrow Mn^{2+}$ redox process improves the electrochemical cyclability. Thus, an optimum potential window between 2.5 and 4.4 V is proposed.

Acknowledgements

The authors acknowledge financial support from the French and Spanish Governments through the PICASSO program (contract HF 1997-0030).

Dr. L. Sánchez also acknowledges the financial support received from Junta de Andalucía Government (Group FQM-175).

References

[1] R.J. Gummow, A. de Kock, M.M. Thackeray, Solid State Ionics 69 (1994) 59.
[2] J.M. Tarascon, W.R. McKinnon, F. Coowar, T.N. Bowmer, G. Amatucci, D. Guyomard, J. Electrochem. Soc. 141 (1994) 1421.
[3] C. Masquelier, M. Tabuchi, K. Ado, R. Kanno, Y. Kobayashi, Y. Maki, O. Nakamura, J.B. Goodenough, J. Solid State Chem. 123 (1996) 255.
[4] J.B. Goodenough, M.M. Thackeray, W.I.F. David, P.G. Bruce, Rev. Chim. Miner. 21 (1984) 435.
[5] W.I.F. David, M.M. Thackeray, L.A. de Piciotto, J.B. Goodenough, J. Solid State Chem. 67 (1987) 316.
[6] T. Tsumura, A. Shimizu, M. Inagaki, Solid State Ionics 90 (1996) 197.
[7] A. Yamada, K. Miura, K. Hinokuma, M. Tanaka, J. Electrochem. Soc. 142 (1995) 2149.
[8] J. Farcy, J.P. Pereira-Ramos, L. Hernán, J. Morales, J.L. Tirado, Electrochim. Acta 39 (1994) 339.
[9] L. Sánchez, J. Farcy, J.P. Pereira-Ramos, L. Hernán, J. Morales, J.L. Tirado, J. Mater. Chem. 6 (1996) 37.
[10] L. Sánchez, J.L. Tirado, J. Electrochem. Soc. 144 (1997) 1939.
[11] L. Sánchez, J. Farcy, J.P. Pereira-Ramos, Electrochim. Acta 43 (1998) 935.
[12] J.M. Jiménez-Mateos, J. Morales, J.L. Tirado, J. Solid State Chem. 82 (1989) 87.
[13] H.P. Klug, L.E. Alexander (Eds.), X-Ray Diffraction Procedures for Polycrystalline and Amorphous Materials, Wiley, New York, 1974, p. 665.
[14] W.R. McKinnon, R.R. Haering, in: R.E. White, J.O.M. Bockris, B.E. Conway (Eds.), Modern Aspects of Electrochemistry, Vol. 15, Plenum Press, New York, 1983.